Creative Commons Attribution

Periodica Polytechnica Civil Engineering, 70(3), pp. 946–957, 2026

Factors Affecting the Dynamic Young's Modulus of Sandstones Using Intelligent and Statistical Methods

Vahid Momeni[1], Mohammad Reza Motahari*[2], Seyed Hamid Lajevardi[3], Hamid Mazaheri[4]

[1] Department of Civil Engineering, Arak Branch, Islamic Azad University, Arak, Iran
[2] Department of Civil Engineering, Faculty of Engineering, Arak University, Arak, Iran
[3] Department of Civil Engineering, Arak Branch, Islamic Azad University, Arak, Iran
[4] Department of Civil Engineering, Khomein Branch, Islamic Azad University, Khomein, Iran
* Corresponding author, e-mail: m-motahari@araku.ac.ir

Received: 06 February 2026, Accepted: 31 July 2026, Published online: 10 September 2026

Abstract

This study analyzed how the sandstone's mineralogy and physical properties affect dynamic Young's modulus (*Ed*). To model these effects, back propagation multilayer perceptron (BPMLP), K-nearest neighbor (KNN), classification and regression tree (CART), simple and multivariate linear regression (MVLR) were employed. After microscopic analysis, compressional and shear wave velocities, water absorption, porosity, and density were measured on the samples. Results showed the calc-litharenite sandstones exhibited a lower *Ed* compared to the feldspathic litharenite types. Quartz showed a stronger influence on *Ed* compared to the porosity and water absorption. A strong correlation between *Es* and *Ed* was proposed. The dynamic modulus was found to exceed the static Young's modulus (*Es*) with a calculated ratio of 2.56 (*Ed* /*Es*=2.56). Based on the RMSE, Nash-Sutcliffe index, *A*20 index, and determination coefficient, the methods were appraised. Within the mineralogical types, quartz had the highest correlation with *Ed*. Mica, opaque, and fragments showed a negative effect on the *Ed*, while chert and cement showed a positive effect on the *Ed*. Among the tested models, BPMLP achieved the highest accuracy, with an *R* of 0.94, RMSE of 0.08, CPM of 1.73GPa, and *A*20 value of 0.98, along with NSE of 97.04%, confirming the superiority of AI-based approaches over statistical techniques in predicting *Ed*.

Keywords

intelligent models, statistical methods, mineralogy, sandstones, static Young's modulus (*Es*), dynamic Young's modulus (*Ed*)

1 Introduction

Dynamic response of rocks is a crucial consideration in numerous geotechnical and civil engineering disciplines, such as tunneling, mining, seismic design, and resource extraction [1]. Gaining a thorough understanding of the variables that influence dynamic Young's modulus (*Ed*) is fundamental to enhancing predictive models and conducting effective hazard evaluations [2]. This literature review aims to explore the body of existing research that addresses the connection between mineralogy and physical properties and their dynamic performance, placing special focus on the use of both statistical techniques and advanced machine learning models.

The dynamic characteristics of rocks are heavily influenced by their physical attributes, including density, porosity, and mineralogical composition. Rocks with higher density typically allow seismic waves to travel faster because of their compact internal arrangement [3]. In contrast, increased porosity generally leads to a decline in wave velocity and *Ed*, as pore spaces hinder efficient wave transmission. The type and proportion of minerals within a rock affect its mechanical response, with each mineral contributing distinct properties such as hardness, elasticity, and resistance to fracturing [4]. Key dynamic parameters like seismic wave velocity, attenuation, and *Ed* provide insight into how rocks behave under mechanical stress. Seismic wave speed reflects both the physical structure and texture of the rock, while attenuation, or the gradual decrease in wave energy, is closely linked to internal features like porosity and grain arrangement [5]. Research by Fereidooni [6] highlighted the influence of mineralogical features and textures on the *Ed* characteristics. Similarly, Hussain et al. [7] used machine learning (ML) approaches to evaluate how variations in mineralogy affect the mechanical behavior of rock aggregates, highlighting the predictive power of mineral composition. Ajalloeian et al. [5]

Cite this article as: Momeni, V., Motahari, M. R., Lajevardi, S. H., Mazaheri, H. "Factors Affecting the Dynamic Young's Modulus of Sandstones Using Intelligent and Statistical Methods", Periodica Polytechnica Civil Engineering, 70(3), pp. 946–957, 2026. https://doi.org/10.3311/PPci.43554

also found that textural elements like intergranular locking and pore geometry significantly affect uniaxial compressive strength (UCS) and *Ed* in carbonate rocks. Khajevand [8] investigated how the petrographic features of carbonate rocks relate to their geotechnical characteristics. By applying empirical modeling techniques, the study demonstrated that porosity is a key factor influencing both strength and elastic properties of these rocks. Ghorbani et al. [9] assessed the impact of detailed textural attributes on hardness, finding that grain dimensions, the degree of cementation, and void arrangement strongly affect the hardness of rock samples.

While numerous studies have developed predictive models for the *Ed*, several limitations remain. Many existing works are confined to localized case studies, limiting their applicability to broader geological contexts [10, 11]. Moreover, some investigations have relied on costly and time-intensive laboratory tests, such as tensile strength measurements, which reduce practicality for widespread application [11]. In other instances, the range of applied predictive techniques has been relatively limited, with only a few models explored [3, 12]. Various intelligent models and empirical relationships have also been evaluated and developed by researchers [13–20]. Table 1 displays some of the models used by different researchers along with their accuracy.

To address these gaps, the current study proposes a comprehensive approach for estimating *Ed* by incorporating multiple modeling techniques and utilizing data from various geological sites. The important point is that the inputs are extracted from non-destructive tests which require very small sample volumes.

The primary objective is to evaluate how variations in physical and petrographic characteristics influence *Ed* using several models. This analysis is conducted through two case studies using both petrographic examinations and a series of engineering tests. Rock samples were gathered from two locations in northern and southern Iran, on which petrographic analysis, measurements of physical properties, and determination of compressional (V_p) and shear wave velocities (V_s) were performed. Subsequently, *Ed* was calculated based on the relevant equation. The study then analyzed how factors such as water absorption, porosity, and the presence of specific rock mineralogy—namely quartz mineral (QuM), feldspar mineral (FelM), and rock fragments (Frs)— affect *Ed*. To model these relationships, back propagation multilayer perceptron (BPMLP), K-nearest neighbor (KNN), classification and regression tree (CART) were employed as intelligent techniques, while simple and multivariate linear regression (MVLR) were applied as statistical methods.

2 Case study

The rock samples examined in this research were collected from the Lar dam region and various mining sites in southern parts of Iran. The dam, standing 105 meters high, is an embankment structure with a clay core, initially designed in 1982. Situated approximately 75 kilometers to the northeast of Tehran, this dam supplies water for agricultural activities and drinking purposes. The Lar dam and its reservoir are located in an area with a complex geological setting, consisting of various formations such as Shemshak, Lar, Laloon, and others. Among these, the Lar and Shemshak formations play a particularly important role in designing engineering projects. The Shemshak formation, which reaches depths greater than 2500 meters in the eastern Alborz zone, dates from the Upper Triassic to the Middle Jurassic periods. The Lar

Table 1 Some of the models used by different researchers along with their accuracy

Authors	Models used	Rock type	Optimum model / Correlation coefficient
Maleki et al. [13]	SVR, BPMLP, GEP	Sedimentary rocks	BPMLP > 0.99
Khosravi et al. [14]	SVR, BPMLP, MVLR	Limestone	SVR: > 0.98
Lawal et al. [15]	GPR, BPMLP, RSM	Various rock types	GPR most accurate
Alizadeh et al. [12]	MVLR, BPMLP	Feldspathic litharenite sandstone	BPMLP: > 95% accuracy
Liu et al. [1]	ANFIS, MVLR, SVR, BPMLP	Sandstone	SVR with $R^2 = 0.98$
Alenizi et al. [10]	GPR, MVLR, BPMLP, KNN	Sandstone and Limestone	GPR most accurate
Yesiloglu-Gultekin and Dogan [16]	GPR, SVR, RT, ET	Basaltic rocks	ET most accurate
Zhang et al. [17]	Not specified	Various rock types	Novel V_p–V_s method for *Es* estimation
Guo et al. [11]	SVR, ANFIS, MVLR, BPMLP	Sedimentary rocks	SVR (RBF kernel): Most accurate
Rezaei et al. [18]	Empirical, MVLR, GEP	Various rock types	GEP: $R^2 > 0.90$
Davarpanah et al. [19]	Empirical models	Various rock types	Improved *Es* prediction using *Ed* and density
Motahari et al. [20]	SVR, MVLR, BPMLP	Sandstone	SVR: $R^2 > 0.98$ for Poisson's ratio and V_s

formation, made up of sedimentary strata up to 483 meters thick, was deposited during the Middle and Upper Jurassic ages. The lithological units of the Shemshak formation serve as the foundation for many key engineering structures in the northern Tehran area and neighboring Alborz Mountain regions. Additionally, the construction of Lar dam faced difficulties due to its foundation on fractured limestone interbedded with sandstone, along with the absence of initial protective works. This makes detailed knowledge of the geological and mechanical properties of these rocks essential.

To ensure a more comprehensive evaluation, additional samples were collected from 10 mining sites situated in southern Iran. The information obtained from these samples, combined with data from the Lar dam area, served as the foundation for developing *Ed* prediction models. The specimens were sourced from active quarries across Bushehr province, with the sandstone, originating from the Aghajari formation. Sandstone rocks are commonly utilized in the construction sector and form the core material for various infrastructure projects such as highways, dams, and tunnels throughout southern Iran. In total, ten active quarries were investigated as part of this research. These mining sites primarily produce various types of rock, including limestone, marl, dolomite, and travertine. Such materials are commonly utilized in construction and form the foundation for numerous engineering works in the region. The Aghajari Formation extends beyond southern Iran into neighboring countries such as Iraq, Syria, and Turkey. It is characterized mainly by continental detrital deposits.

3 Materials and methods

3.1 Rock mechanics tests

In this study, the dynamic, physical, and mineralogical properties of 91 sandstone samples from the Lar dam site and southern Iranian mines were measured. Discontinuities cause asymmetric stresses and errors in measuring the elastic modulus and strength of the samples [1, 7]. Hence, the samples used in the present study are free of joints and cracks.

Table 2 outlines the primary standards and procedures applied in carrying out the rock mechanics experiments [21–25]. Once the specimens were prepared, they first underwent non-destructive testing, including measurements of compressional wave velocity (V_p) and shear wave velocity (V_s). This was followed by physical property assessments, covering parameters such as porosity, density, and water absorption. The thin section and X-ray diffraction (XRD) were used to precisely determine their lithological composition.

$$Ed = \frac{\rho \times V_s^2 \left(3V_p^2 - 4V_s^2\right)}{V_p^2 - V_s^2} \tag{1}$$

3.2 CART methodology

In the case of regression, the CART objective is to reduce the variance within these groups as much as possible. The algorithm builds a hierarchical tree by dividing the dataset at each node using an optimal split, which in this study is based on the least square deviation (LSD) criterion. After constructing the full tree, it is often necessary to prune it to enhance simplicity and prevent overfitting. For regression purposes, the output for any input record corresponds to the mean value of the target variable within the leaf node where that record ends up, as described in Eq. (2) [26].

$$D(t) = \sum_{i=1}^{Ntt} \left(o_i(t) - \bar{o}(t)\right)^2 \tag{2}$$

In this context, $D(t)$ indicates the criterion applied to form branches and develop decision trees. The term Nt refers to the number of data samples contained in leaf node t, and o_i represents the output associated with each sample. The symbol $\bar{O}(t)$ corresponds to the mean output value across all nodes. The value Dt is regarded as the best split point at node t when it leads to the highest $Q(d,t)$ score, as outlined in Eq. (3).

$$Q(d,t) = D(t) - D(tR) - D(tL) \tag{3}$$

Here, D(tR) and $D(tL)$ indicate the values of $D(t)$ corresponding to the right and left child branches of node t, respectively.

Table 2 Instructions for measuring mineralogical and physical properties and Young's modulus

Test type	Parameters measured
Thin section and XRD analysis	Rock type determined according to classifications by Folk [21]
Physical properties test [22]	Measured properties: water absorption (W, %), porosity (n, %), and density (ρ, g/cm^3)
Uniaxial compressive strength (UCS) [23]	To determine the elasticity modulus (Es), the slope of the stress-strain curve in the uniaxial compressive strength (UCS) test was used [23]. The calculated modulus of elasticity is tangential. In this way, at 50% of the UCS, a tangent line is formed and the slope of that line is equivalent to the tangent modulus of elasticity.
Dynamic properties test (ASTM D2845) [24]	Determined values: compressional and shear wave velocities (V_p, V_s, km/s), dynamic Young's modulus (Ed, GPa), calculated using Eq. (1), [25].

The Gini index (*GI*), defined in Eq. 4, measures how similar the data points are within each node. In regression trees, the aim is to reduce the *GI* at each split to create more uniform nodes, thereby boosting prediction accuracy.

$$GI = 1 - \sum_{i=1}^{n} \left(p_i^2 \right) \tag{4}$$

In this context, n denotes the total number of unique classes, while p_i indicates the fraction of samples in the node that belong to class i compared to the overall sample count.

3.3 BPMLP methodology

In this study, a BPMLP method was used for forecasting the *Ed* based on measured physical and mineralogical parameters. BPMLP is a type of artificial neural network (ANN) composed of an input layer, one or more hidden layers, and an output layer. The model learns the relationship between inputs and outputs through a training process based on the back propagation algorithm, which iteratively adjusts the internal weights to minimize the prediction error. BPMLP belongs to the category of feedforward neural networks. In this type of network, information transfers in one direction: from the input layer to the output layer, passing through one or more hidden layers. Several formulas, drawn from different studies, can be applied to estimate the appropriate number of neurons for testing [27]. These formulas helped define the neuron range assessed in this work. For training the BPMLP, the Levenberg-Marquardt (LM) technique was utilized. The BPMLP method has been fully explained and described by the authors [20, 27, 28].

K-nearest neighbor (KNN) methodology has been explained by various scholars [10, 15, 29]. In all used methods, the dataset was randomly partitioned so that threequarters were used to train the models, while the remaining onequarter served for testing. The data was also normalized between −1 and 1 for modeling. The overfitting occurrence of the models was controlled by model accuracy in the training and testing phases.

3.4 Evaluating metrics

Model performance in estimating *Ed* was evaluated using a suite of statistical metrics—coefficient of determination (R^2), rootmeansquare error (RMSE), Nash–Sutcliffe efficiency (NSE), variance accounted for (VAF), computed performance metric (CPM), and *A*20 index–derived via Eqs. (5–9). A superior model exhibits higher R^2, NSE, and *A*20 index values alongside a lower RMSE.

$$\mathrm{RMSE} = \sqrt{\frac{1}{N} \sum_{i=1}^{N} \left(Ed - Ed' \right)^2} \tag{5}$$

$$\mathrm{NSE} = 1 - \left(\frac{\sum_{i=1}^{N} \left(Ed - Ed' \right)^2}{\sum_{i=1}^{N} \left(Ed - \overline{Ed} \right)^2} \right) \tag{6}$$

$$A20 \text{ index} = \frac{\left(\frac{Ed}{Ed'} \right)_{20}}{N} \tag{7}$$

$$\mathrm{VAF} = 1 - \left(\frac{\mathrm{Var}\left(Ed - Ed' \right)}{\mathrm{var}\left(Ed \right)} \right) \tag{8}$$

$$\mathrm{CPM}\left(\mathrm{GPa} \right) = \mathrm{VAF} + R^2 - \mathrm{RMSE} \tag{9}$$

Where *Ed* denotes the experimentally determined elastic Young's modulus, *Ed*' represents the model's predicted elastic Young's modulus, $\overline{Ed}$ is the mean of the observed *Ed* values, and N is the total sample count. The *Ed* / *Ed*' counts how many predictions fall within 80–120%.

To develop the models using MATLAB software [30] and by the trial-and-error method, the test and train data were randomly divided. 75% of the data was allocated for training purposes, and the remaining 25% was allocated for testing the models.

4 Results and discussions

4.1 Samples' classification

Petrographic analysis plays a crucial role not only in identifying the mineral content and geological origin of rocks but also in assessing their mechanical behavior and susceptibility to weathering [31, 32].

In this study, a total of 91 thin sections were prepared and analyzed from rock samples collected at the studied sites. The investigation focused on identifying the mineral composition and textural attributes of the sandstone samples using both petrographic thin section analysis and X-ray diffraction (XRD). Microscopic examination revealed that the sandstones consist primarily of carbonate minerals, quartz, chert, schist, feldspar, and iron oxide. Based on Folk's [21] classification, the sandstones from the Aghajari Formation are categorized as calc-litharenite, while those from the Shemshak Formation fall under feldspathic litharenite (Table 3).

Thin section observations further indicated that Aghajari sandstones are composed of quartz, carbonates, feldspar, schist, iron oxides, and are cemented with calcite, clay, and gypsum. The average size of carbonate grains across all samples ranged from 0.2 to 0.5 mm. Calcite is the dominant cementing material in Aghajari sandstones, often creating localized connections between grains. Clay and gypsum cements were also identified. The sandstone grains were semi-rounded and exhibited variable degrees of dissolution.

Table 3 The geological characteristics of the samples analyzed in the present study

Project	Sandstone types	Used samples	Depth (m)	Formation	Age
Lar dam site	Feldspathic litharenite (FLA)	56	1.00–45.60	Shemshak	Jurassic
Mines	Calc-litharenaite (CLA)	35	2.60–39.50	Aghajari	Miocene to Pliocene

Cement types differ between the formations: Aghajari sandstones predominantly contain calcite, gypsum, and clay cements, while siliceous cement is more common in the Shemshak Formation. Lithic fragments from Aghajari are mostly carbonate-based, whereas those from Shemshak include chert and opaque minerals.

Mineralogical compositions were further validated through XRD analysis. Silica cement tends to create strong intergranular bonds, enhancing mechanical strength. Although calcite cement can also provide considerable strength, it is vulnerable to pressure dissolution, which may reduce rock durability over time. As a result, *Ed* values can range from moderate to high depending on mineral presence. Iron oxide cement exhibits variable effects: hematite contributes positively to strength, while other iron oxides may reduce it. Thus, mechanical behavior is influenced by the type and proportion of iron oxides [32, 33].

4.2 Characteristics of samples

The mineralogy and geo-mechanical characteristics of sandstone rocks, as presented in Table 4, reveal considerable variability across the samples. The *Ed*, representing the stiffness of the rock, varies significantly between 21.64 and 95.49 GPa, with an intermediate mean value of 49.35 GPa. This indicates the presence of both relatively soft and very stiff sandstone units. This variability suggests differences in diagenetic history and bonding strength among the sandstone veins. In summary, calc-litharenite sandstones have a lower *Ed* than feldspathic litharenite. Also, the percentage of quartz in the sandstones of southern Iran (calc-litharenite sandstones) is lower than that of the sandstones from the Lar dam (feldspathic litharenite). Based on the Anon [34] and ISRM [22] classifications, the samples are classified into the low category based on porosity.

4.3 The effect of minerals and sandstone types on Young's modulus

The type and amount of minerals affect the mechanical properties [31, 32]. Fig. 1 illustrates the relationship between mineral and the Young's modulus (*Ed*) of two types of sandstone: feldspathic litharenite (FLA) and calc-litharenite (CLA) for 17 samples. In general, FLA samples tend to exhibit higher Young's modulus values (up to 78.63 GPa) compared to CLA samples (mostly below 56 GPa), indicating stiffer and potentially more competent rock. FLA samples also show higher percentages of quartz and feldspar and lower percentages of rock fragments, which aligns with higher *Ed* values. Conversely, CLA samples with higher amounts of rock fragments and lower quartz content generally correspond to lower Ed, suggesting that increased fragment content reduces the rock's stiffness. Thus, mineralogical composition, particularly higher quartz and feldspar and reduced rock fragments, appears to significantly enhance the mechanical stiffness of sandstones. As previously mentioned, the sandstones of the Lar dam site are of the feldspathic litharenite type, and the sandstones of the southern mines are of the calc-litharenite type. As will be presented below (the correlation matrix of the variables), minerals like mica, chert, and opaque phases have comparatively minor roles, with only weak correlations to *Ed*, indicating a limited contribution to rock rigidity. Previous studies have confirmed that quartz plays a key role in improving the uniaxial compressive strength and elasticity of rocks, whereas feldspar tends to reduce these mechanical properties [12].

Table 4 The Mineralogy and geo-mechanical characteristics of the samples

	Wa %	P %	*Ed* (GPa)	*Es*(GPa)	QuM %	Frs %	FelM %	Chert %	Opaque %	Mica %	Cement %
Mean	2.31	4.26	49.35	19.64	15.44	38.99	43.55	1.17	5.32	1.19	8.94
Standard error	0.23	0.33	1.92	0.72	0.22	0.63	0.35	0.11	0.36	0.12	0.71
Sample variance	4.75	10.12	334.76	47.26	4.53	35.91	11.10	0.39	4.21	0.48	16.47
Kurtosis	(0.83)	(0.49)	(0.32)	(1.05)	(1.00)	(1.01)	(0.96)	(0.42)	(0.69)	(0.85)	3.87
Skewness	0.69	0.49	0.60	0.04	0.10	(0.11)	0.14	0.09	0.20	0.14	2.03
Minimum	0.01	0.00	21.64	5.60	11.52	26.72	37.48	0.30	2.30	0.30	4.30
Maximum	8.00	13.00	95.49	32.00	19.83	49.91	50.45	2.30	9.30	2.30	20.30

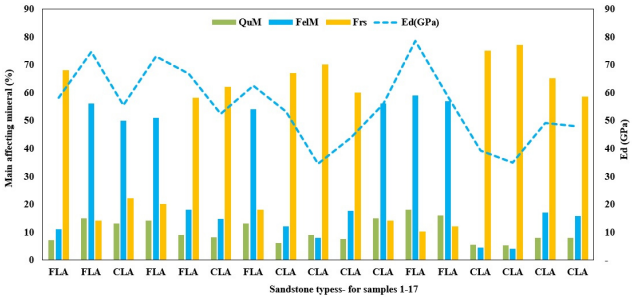

Fig. 1 The relationship between mineral composition (quartz mineral [QuM], feldspar mineral [FelM], and rock fragments [Frs]) and the dynamic Young's modulus (*Ed*) of two types of sandstone: feldspathic litharenite (FLA) and calc-litharenite (CLA) for 17 samples

4.4 *Ed* and *Es* relationship, *Ed* /*Es* ratio, and efficiency of previous relationships

Because obtaining direct measurements is often expensive and limited by sample availability, using predictive equations to estimate *Es* has become a practical alternative. As displayed in Fig. 2, there is a meaningful relationship between *Es* and *Ed*. Among the types of fits studied to determine the relationship between these two variables, the linear, power, and logarithmic relationships have the highest accuracy (Fig. 2). The aforementioned relationships have been evaluated based on various metrics and Taylor [35] classification (Table 5). The evaluations show that these relationships can be used with very high accuracy to estimate the *Es* in the identification phase of civil and mining projects.

$$Es = 0.33Ed + 3.54 \tag{10}$$

$$Es = 16.35Ln\left(Ed\right) - 42.98 \tag{11}$$

$$Es = 0.53Ed^{0.93} \tag{12}$$

The results of the present study showed that the ratio of dynamic to static modulus for all samples is 2.56

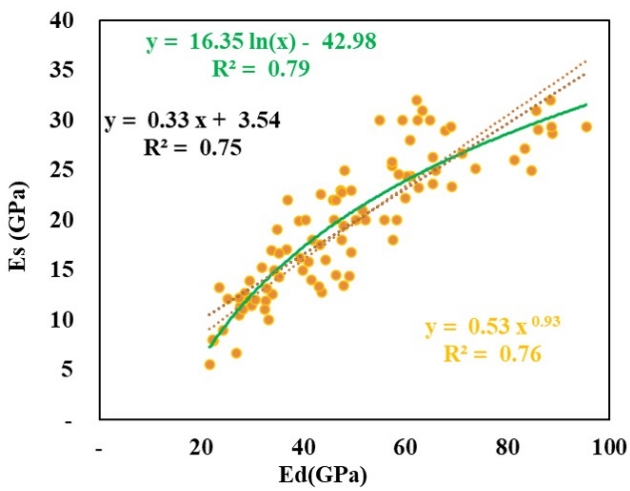

Fig. 2 *Ed* and *Es* relationship

Table 5 Performance of statistical criteria for evaluating the relationship between static and dynamic modulus

Eqs.	R^2	Taylor [35] classification	RMSE	VAF	CPM (GPa)	*A*20	NSE
(10)	0.75	Strong correlation	0.28	0.74	1.21	0.97	0.94
(11)	0.79	Strong correlation	0.25	0.78	1.32	0.98	0.95
(12)	0.76	Strong correlation	0.30	0.75	1.21	0.97	0.96

(*Ed*/*Es*=2.56). The detailed results of the studies showed that the amount of this ratio is strongly dependent on the types of sandstone samples. Calc-litharenite types have a mean ratio of 3.94 and feldspathic litharenite samples have a mean ratio of 1.70. The minimum and maximum values of the *Ed*/*Es* ratio for the Calc-litharenite samples are 3.49 and 5.08, while for the feldspathic litharenite samples, the minimum and maximum *Ed*/*Es* ratios are 1.40 and 2.12. The *Ed*/*Es* ratio variance values are 0.13 and 0.05 for Calc-litharenite and feldspathic litharenite samples, respectively. Therefore, the *Ed*/*Es* ratio is larger in weaker samples as compared with stronger samples. As previously mentioned, the density and *Es* of felspathic litharnite samples (sandstones from the Lar Dam construction site) are higher than those of calc-litharnite samples (sandstones from the southern Iranian mines). Also, the porosity and clay minerals in the sandstone samples from the Lar dam site were lower than those in the sandstone samples from the southern Iranian mines. Similar results have been reported in previous research, indicating that these two moduli are not equivalent, and the dynamic modulus generally yields higher values than the static modulus [10, 17]. Several factors contribute to these differences, including the anisotropic characteristics of rocks, pore fluid presence, variations in strain magnitude, existing cracks, porosity levels, and the degree of cementation within samples [10, 25]. Among these, the strain magnitude is considered the primary reason for the discrepancy between dynamic and static moduli, rather than the strain rate [32]. Because static modulus is derived from the slope of the stress–strain curve and is influenced by plastic deformation, it differs from the dynamic modulus measured at minimal strain ranges [25].

For example, Fig. 3 presents an evaluation of the applicability of previously proposed equations (listed in Table 6) for predicting *Es* [1, 3, 10, 11, 14, 19, 20, 31, 33, 36–39]. In this assessment, *Es* was estimated for each sample using these earlier equations, and the calculated values were then compared with the corresponding laboratory measurements

obtained in the present study. In this analysis, equations relevant to the lithologies investigated here were assessed. The results demonstrated a strong correlation (R^2 > 68%) between the measured *Es* values and some of the predicted results, indicating generally good agreement. Despite this, the very low CPM values reveal that these earlier equations are not particularly effective in accurately estimating the *Es* of the studied samples.

$$Es = 0.42Ed \tag{13}$$

$$Es = 0.73 + 0.42Ed \tag{14}$$

$$Es = 0.70Ed + 2.05 \tag{15}$$

$$Es = 0.41Ed - 0.93 \tag{16}$$

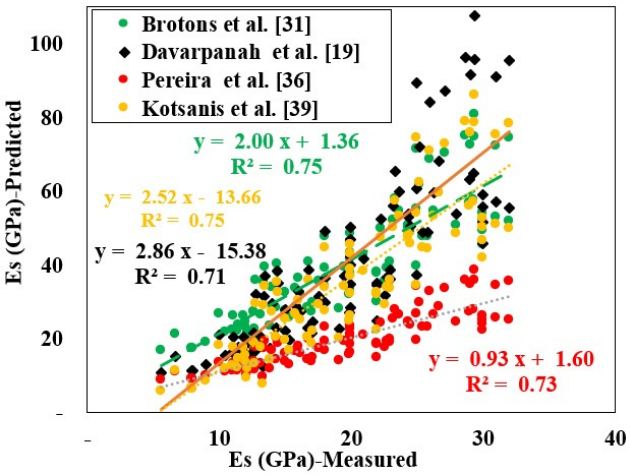

Fig. 3 An example of the measured static modulus relationship with estimated based on previous relationships

Table 6 Previous researchers' relationships for estimating static modulus based on dynamic modulus

Eq. No.	Lithology type	Reference
(13)	Igneous rocks	Pereira et al. [36]
(14)	Sandstone samples	Motahari et al. [20]
(15)	Mixed lithologies	Onaloa et al. [37]
(16)	Sedimentary samples	Alenizi et al. [10]
(17)	Sandstones	Liu et al. [1]
(18)	Various rock types	Brotons et al. [31]
(19)	Different lithologies	Davarpanah et al. [19]
(20)	Multiple rock classes	Brotons et al. [33]
(21)	Siliceous formations	Fei et al. [38]
(22)	Limestone samples	Ghafoori et al. [3]
(23)	Carbonate rocks	Khosravi et al. [14]
(24)	Prasinite lithologies	Kotsanis et al. [39]
(25)	Sedimentary types	Guo et al. [11]

$$Es = 1.87 + 0.37Ed \tag{17}$$

$$Es = 0.87Ed - 2.05 \tag{18}$$

$$Es = 0.091Ed \wedge 1.552 \tag{19}$$

$$Es = 0.90Ed - 3.35 \tag{20}$$

$$Es = 0.60Ed - 3.45 \tag{21}$$

$$Es = 0.02Ed \wedge 1.80 \tag{22}$$

$$Es = 0.03Ed \wedge 1.80 \tag{23}$$

$$Es = 1.15Ed - 17.95 \tag{24}$$

$$Es = 2.13Ed \wedge 0.54 \tag{25}$$

4.5 Checking normality, correlation matrix, and outliers of data for *Ed* modeling

According to Grubbs' outlier test at a 5% significance level, no significant outliers were identified in any of the variables affecting Young's modulus.

The analysis reveals that *Ed* is strongly influenced by mineralogical and physical characteristics (Fig. 4). Specifically, it exhibits a strong positive correlation with quartz mineral (QuM) and feldspar mineral (FelM), indicating that higher contents of these components enhance the rock's stiffness. In contrast, porosity, fragments (Frs), and water absorption show strong negative correlations with *Ed*, suggesting that increased pore space and moisture content significantly reduce *Ed*. Carbonate and gypsum fragments were the dominant percentage of the rock fragments in the studied samples. The negative relationship between *Ed* and Frs indicates that these rock fragments cause a decrease in the dynamic modulus. Thin section examination of the studied sandstones showed that these rocks are composed of carbonate fragments, gypsum fragments, volcanic fragments, metamorphic fragments, quartz, chert, dark minerals and feldspar. Minor components such as muscovite and clay fragments are also visible in some samples.

Based on Taylor [35] classification, QuM, Frs, FelM, porosity, and water absorption can be used to estimate *Ed* because they have correlation coefficients higher than 0.70. Table 7 shows the performance of different statistical measures for the influence of physical and mineralogical properties on dynamic modulus.

$$Ed = 108.93e^{-0.148Wa} \tag{26}$$

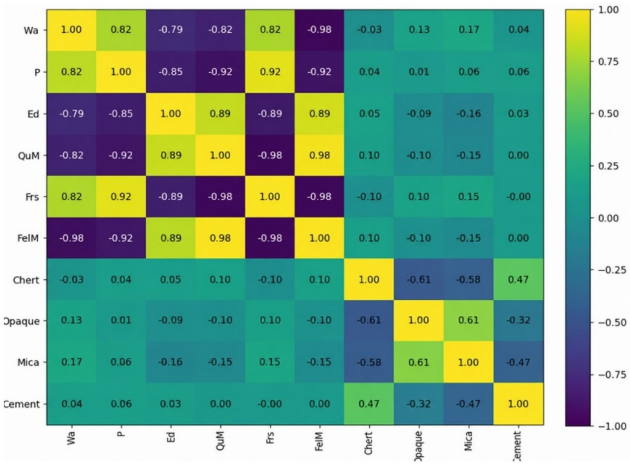

Fig. 4 Correlation matrix of variables: *Ed*, minerals, and physical properties

$$Ed = -4.90P + 70.22 \tag{27}$$

$$Ed = 7.51QuM - 66.59 \tag{28}$$

$$Ed = 4.75FelM - 157.75 \tag{29}$$

$$Ed = -2.70Frs + 154.71 \tag{30}$$

4.6 MVLR Analysis

The final MVLR model incorporates three predictors: water absorption (*Wa*), porosity (*P*), and quartz mineral (*QuM*). Two others initially considered variables—feldspar mineral (*FelM*) and rock fragments (*Frs*)—were excluded from the model, due to either statistical insignificance or multicollinearity with the included variables. The regression equation derived from the analysis is:

$$Ed = -9.80 - 1.53Wa - 1.32P + 4.43QuM \tag{31}$$

This equation reveals that both water absorption and porosity have negative coefficients, indicating that increases in these parameters lead to decreases in Young's modulus. This relationship is geomechanically sound, as rocks with higher porosity and water content generally possess weaker internal bonding and reduced stiffness. In contrast, the quartz content exerts a strong positive effect on *Ed*, underscoring the role of quartz's high hardness and rigidity in enhancing the elastic modulus of the rock.

Table 7 Bivariate relationships between the dynamic model and physical and mineralogical properties

Eq.	R^2	Taylor [35] classification	RMSE	VAF	CPM	*A*20	NSE%
(26)	0.73	Strong correlation	0.31	0.72	1.16	0.95	0.89
(27)	0.73	Strong correlation	0.29	0.72	1.22	0.94	0.85
(28)	0.76	Strong correlation	0.27	0.75	1.24	0.98	0.85
(29)	0.75	Strong correlation	0.29	0.74	1.20	0.96	0.91
(30)	0.78	Strong correlation	0.31	0.77	1.24	0.95	0.90

The model demonstrates strong performance in predicting *Ed* values. However, the variance inflation factor (*VIF*) for porosity, exceeding 7, points to moderate multicollinearity; while not severe, it could slightly impact the reliability of coefficient estimates (Table 8). Analysis of variance showed that the fitted model is appropriate because of a *p*-value of 0.00.

4.7 BPMLP model results

In this study, the optimal number of neurons in the hidden layer for predicting *Ed* using BPMLP, a type of artificial neural network, was determined based on both established empirical formulas and experimental testing. Initial estimates were informed by earlier research recommendations, suggesting the use of 1 to 9 neurons [27]. However, to improve the reliability of the results and allow for a more comprehensive performance evaluation, the neuron count was extended up to 16 through a trial-and-error process. The BPMLP architecture consisted of a single hidden layer, with three inputs and *Ed* as the target output. The input layer included 3 neurons corresponding to the 3 predictor variables. The hidden layer used the PureLin activation function, while the Sigmoid function was used in the output layer. The hidden layer with a linear activation preserves the linear relationships among the extracted features without introducing additional nonlinear distortions, while the sigmoid output layer maps the network output to a bounded range, making it suitable for prediction tasks requiring normalized outputs. This configuration was selected based on preliminary experiments that demonstrated satisfactory convergence and predictive performance for the proposed model. Various hidden layer configurations were examined, and the model with a third hidden neuron delivered the best performance, achieving the highest correlation coefficient with the observed *Ed* values and the lowest prediction error.

Fig. 5 displays the correlation results between *Ed* and the input variables across various datasets, generated using optimized BPMLP models trained with the Levenberg-Marquardt (LM) algorithm. These visualizations confirm the high predictive accuracy of the developed models. Usually, the validation set is used to prevent overfitting, the training

Table 8 Characteristics of the MVLR model

Term	Coef	SE Coef	*T*-value	*P*-value	VIF
Constant	−9.8	20.3	−0.49	0.028	–
Wa	−1.527	0.750	−2.04	0.04	3.29
P	−1.318	0.765	−1.72	0.03	7.28
QuM	4.43	1.12	3.95	0.000	6.99

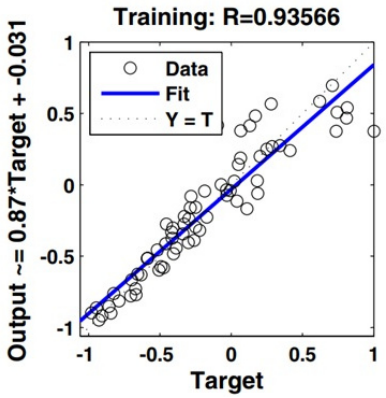

(a)

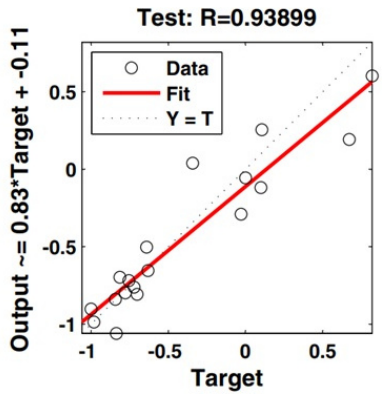

(b)

Fig. 5 Correlation results between *Ed* and the input variables using the BPMLP model: (a) for the training data set; (b) for the test data set

group is used to determine weights, and the test group is used to evaluate the BPMLP results [28]. Since the results of the train and test data are almost equal, it can be stated that the developed BPMLP model is not overfitted. The very closeness of the correlation coefficient of the validation set (R=0.94) to the test and training sets also showed that the model has optimal accuracy. Fig. 6 demonstrates the trend of error reduction during the LM training process within the best-performing model. The lowest prediction error for *Ed* was achieved at epoch 10.

4.8 CART modeling results

The CART method used least squares error for node splitting, and the optimal tree was selected based on the R-squared value within one standard error of the maximum. The tree

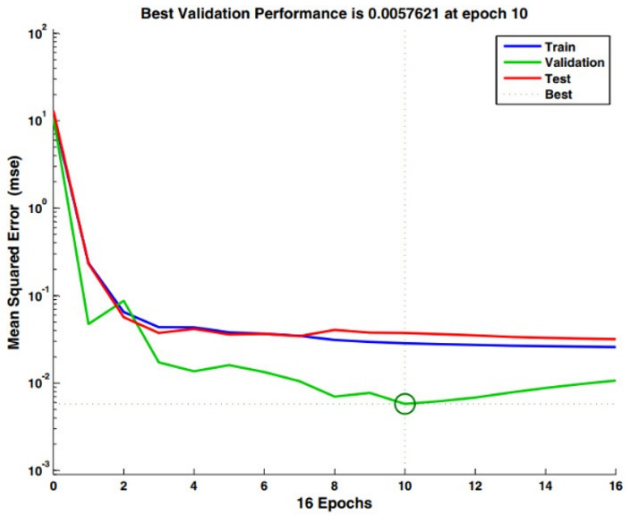

Fig. 6 Error change trend for estimating *Ed* using BPMLP model

structure revealed that the first split is made based on quartz content (QuM), indicating its dominant role in controlling *Ed*. Subsequent splits involve *Wa* and *P*, reflecting their secondary influence. Fig. 7 shows CART methodology used in current study. The training dataset yielded a high R-squared value of 82.59%, while the test dataset achieved a respectable R-squared of 68.64%, confirming good generalizability and predictive accuracy (Table 9).

4.9 KNN models

The KNN approach relies on a distance metric to identify the most relevant nearby instances. In this study, Euclidean distance was selected for forecasting *Ed* values. As illustrated in Fig. 8, training errors fluctuate with varying K values, and the lowest prediction error for *Ed* was achieved when K was set to 4. The equal accuracy of the test data and model testing results showed that the models were not overfitted.

4.10 Comparing modeling results and determining the optimal model

The performance of different methods using different criteria is presented in Table 9 to compare the models and suggest the optimal model. As can be seen, the BPMLP method shows better superiority over other methods in estimating *Ed*. This conclusion is based on the evaluation of several statistical criteria. Also, in general, it can be stated that the ML methods offer greater superiority over the MVLR method. One of the main strengths of ML methods is their ability to model nonlinear relationships. Another key benefit is the relaxed requirement for statistical assumptions. While classical methods typically depend on conditions like normality checking, independence of parameters, and multicollinearity, ML techniques can function effectively

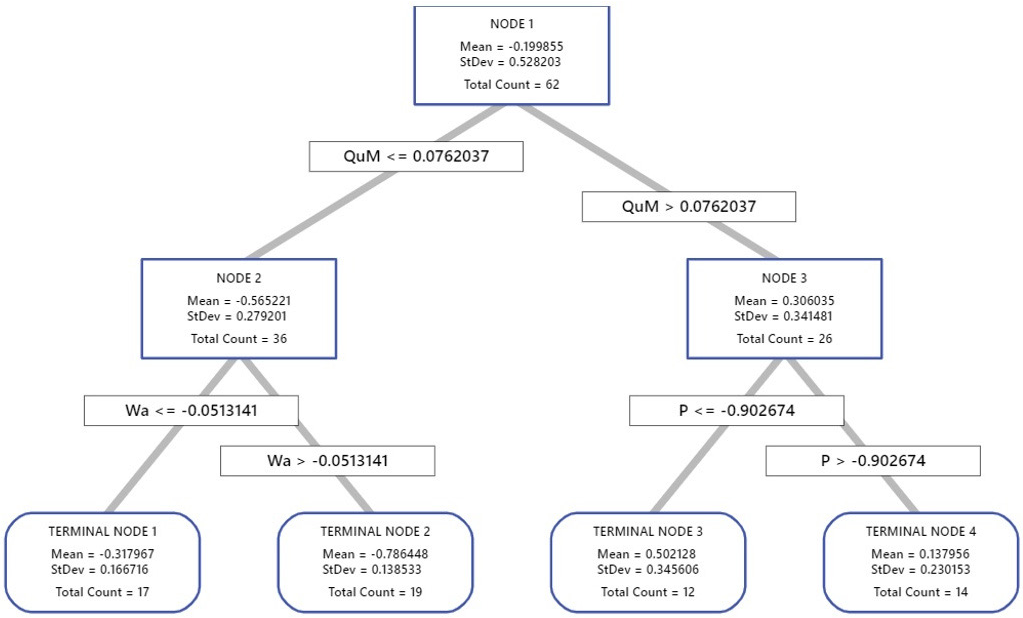

Fig. 7 Used CART methodology for estimating *Ed*

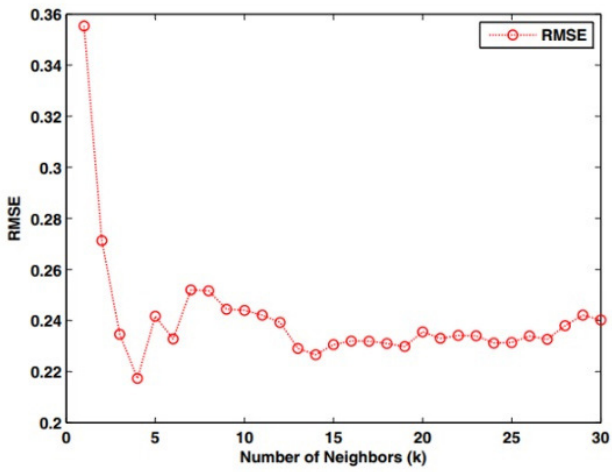

Fig. 8 RMSE for different *K* using KNN model

without these constraints, making them more suitable for real-world datasets [40, 41].

5 Conclusions

In the present research, different approaches, including statistical methods as well as *K*-nearest neighbor (KNN), multivariate linear regression (MVLR), classification and regression tree (CART), and backpropagation multilayer perceptron (BPMLP), were applied to predict the dynamic Young's modulus (*Ed*) of sandstone samples based on quartz, feldspar, fragments, porosity, and water absorption from the Lar dam and mine sites. Petrographic studies under the microscope classified the rock specimens, such as calc-litharenite and feldspathic litharenite based on thin sections and XRD. The sandstones of the Lar dam site are of the feldspathic litharenite type, and the sandstones of the Bushehr mines in southern Iran are of the calc-litharenite type. Calc-litharenite sandstones showed a lower *Ed* than feldspathic litharenite. Also, the percentage of quartz in the sandstones of southern Iran (calc-litharenite sandstones) is lower than that of the sandstones from the Lar dam (feldspathic litharenite).

A strong correlation between *Es* and *Ed* was proposed. The dynamic modulus was found to exceed the static modulus, with a calculated ratio of 2.56 (*Ed* /*Es*=2.56) for all samples. Among the sandstone types, calc-litharenite types showed a ratio of 3.94, while feldspathic litharenite samples displayed a ratio of 1.70. In general, weak samples showed a greater *Ed*/*Es* ratio than stronger samples. The MVLR regression model confirms that quartz content is the most influential and statistically reliable factor affecting dynamic Young's modulus

Table 9 The performance of statistical criteria in identifying the optimal model for estimating *Ed* based on test set

Used methods	*R*	Taylor [35] classification	RMSE (GPa)	VAF	CPM (GPa)	*A*20	NSE%
BPMLP	0.94	Strong	0.08	0.93	1.73	0.98	97.04
KNN	0.89	Strong	0.21	0.88	1.46	0.95	92.27
CART	0.83	Strong	0.22	0.83	1.30	0.94	92.20
MVLR	0.89	Strong	0.32	0.87	1.34	0.91	90.55

among the variables considered. While water absorption and porosity negatively correlate with *Ed*, their roles are less definitive, particularly for porosity.

The results highlight the benefits of utilizing intelligent algorithms, which surpass the accuracy of conventional multivariable linear regression models in forecasting *Ed*. Among the evaluated techniques, BPMLP stands out with the highest accuracy, supported by statistical indicators such as a correlation coefficient of 0.94, RMSE of 0.08GPa, CPM=1.73, Nash-Sutcliffe index of 97.04%, and *A*20 index of 0.98.

The results demonstrated a practical approach for selecting the most suitable machine learning techniques to accurately forecast the *Ed* of rocks, offering valuable support during site investigations in civil and mining projects. Since the results of the test and training data are almost equal, there is no overfitting in the models. Therefore, it is recommended that the models and correlations developed in this work show potential for partial application to other areas, as they were formulated across a range of input values.

References

[1] Liu, N., Sun, Y., Wang, J., Wang, Z., Rastegarnia, A., Qajar, J. "Estimation of static Young's modulus of sandstone types: effective machine learning and statistical models", Earth Science Informatics, 17, pp. 4339–4359, 2024. https://doi.org/10.1007/s12145-024-01392-6

[2] Xie, Y., Wang, L., Gu, Y., Gu, X., Chen, S., Khajehzadeh, M., Hosseini, S. "Prediction of Rock's Brittleness and Dynamic Properties Utilizing Effective Artificial Intelligence Approaches", Periodica Polytechnica Civil Engineering, 68(3), pp. 946–960, 2024. https://doi.org/10.3311/PPci.23156

[3] Ghafoori, M., Rastegarnia, A., Lashkaripour, G. R. "Estimation of static parameters based on dynamical and physical properties in limestone rocks", Journal of African Earth Sciences, 137, pp. 22–31, 2018. https://doi.org/10.1016/j.jafrearsci.2017.09.008

[4] Lu, J., Liao, X., Rastegarnia, A., Qajar, J. "Estimating UCS of South China sandstones using mineralogical and machine learning approaches", Physics and Chemistry of the Earth, Parts A/B/C, 141, 104048, 2025. https://doi.org/10.1016/j.pce.2025.104048

[5] Ajalloeian, R., Mansouri, H., Baradaran, E. "Some carbonate rock texture effects on mechanical behavior, based on Koohrang tunnel data, Iran", Bulletin of Engineering Geology and the Environment, 76(1), pp. 295–307, 2017. https://doi.org/10.1007/s10064-016-0861-y

[6] Fereidooni, D. "Importance of the mineralogical and textural characteristics in the mechanical properties of rocks", Arabian Journal of Geosciences, 15(7), 637, 2022. https://doi.org/10.1007/s12517-022-09929-z

[7] Hussain, J., Zafar, T., Fu, X., Ali, N., Chen, J., Frontalini, F., Hussain, J., Lina, X., Kontakiotis, G., Koumoutsakou, O. "Petrological controls on the engineering properties of carbonate aggregates through a machine learning approach", Scientific Reports, 14, 31948, 2024. https://doi.org/10.1038/s41598-024-83476-3

[8] Khajevand, R. "Evaluating the influence of petrographic and textural characteristics on geotechnical properties of some carbonate rock samples by empirical equations", Innovative Infrastructure Solutions, 6(2), 113, 2021. https://doi.org/10.1007/s41062-021-00498-w

[9] Ghorbani, S., Hoseinie, S. H., Ghasemi, E., Sherizadeh, T. "Effect of quantitative textural specifications on Vickers hardness of limestones", Bulletin of Engineering Geology and the Environment, 82(1), 32, 2023. https://doi.org/10.1007/s10064-022-03049-4

[10] Alenizi, F. A., Mohammed, A. H., Alizadeh, S. M., Gohari, O. M., Motahari, M. R. "Appraisal of rock dynamic, physical, and mechanical properties and forecasting shear wave velocity using machine learning and statistical methods", Journal of Applied Geophysics, 223, 105216, 2024. https://doi.org/10.1016/j.jappgeo.2023.105216

[11] Guo, S., Zhang, Y., Iraji, A., Gharavi, H., Deifalla, A. F. "Assessment of rock geomechanical properties and estimation of wave velocities", Acta Geophysica, 71(2), pp. 649–670, 2023. https://doi.org/10.1007/s11600-022-00891-8

[12] Alizadeh, S. M., Iraji, A., Tabasi, S., Ahmed, A. A. A., Motahari, M. R. "Estimation of dynamic properties of sandstones based on index properties using artificial neural network and multivariate linear regression methods", Acta Geophysica, 70(1), pp. 225–242, 2022. https://doi.org/10.1007/s11600-021-00705-3

[13] Maleki, S., Ramazi, H. R., Shahrabi, M. A. "Application of artificial intelligence techniques in the estimation of Young's modulus by conventional well logs", International Journal of Engineering Science, 16(1), pp. 49–58, 2024. https://doi.org/10.57647/j.ijes.2024.1601.04

[14] Khosravi, M., Tabasi, S., Eldien, H. H., Motahari, M. R., Alizadeh, S. M. "Evaluation and prediction of the rock static and dynamic parameters", Journal of Applied Geophysics, 199, 104581, 2022. https://doi.org/10.1016/j.jappgeo.2022.104581

[15] Lawal, A. I., Kwon, S., Aladejare, A. E., Oniyide, G. O. "Prediction of the static and dynamic mechanical properties of sedimentary rock using soft computing methods", Geomechanics and Engineering, 28(3), pp. 313–324, 2022. https://doi.org/10.12989/gae.2022.28.3.313

[16] Yesiloglu-Gultekin, N., Dogan, A. "Estimation of the elastic modulus of basaltic rocks using machine learning methods", Earth Science Informatics, 17(6), pp. 5941–5966, 2024. https://doi.org/10.1007/s12145-024-01472-7

[17] Zhang, Y., Gu, Y., Zhou, H., Yang, L. "Extracting static elastic moduli of rock through elastic wave velocities", Acta Geophysica, 72(2), pp. 915–931, 2023. https://doi.org/10.1007/s11600-023-01139-9

[18] Rezaei, M., Ahmadi, S. R., Nguyen, H., Armaghani, D. J. "Improved determination of the S-wave velocity of rocks in dry and saturated conditions: Application of machine-learning algorithms", Transportation Geotechnics, 49, 101371, 2024. https://doi.org/10.1016/j.trgeo.2024.101371

[19] Davarpanah, S. M., Ván, P., Vásárhelyi, B. "Investigation of the relationship between dynamic and static deformation moduli of rocks", Geomechanics and Geophysics for Geo-Energy and Geo-Resources, 6(1), pp. 29, 2020.
https://doi.org/10.1007/s40948-020-00155-z

[20] Motahari, M. R., Amini, O., Iraji, A., Gohari, O. M., Saffarian, M. "Comparison of dynamic and static properties of sandstone and estimation of shear wave velocity and Poisson's ratio", Bulletin of Engineering Geology and the Environment, 81(9), 384, 2022.
https://doi.org/10.1007/s10064-022-02867-w

[21] Folk, R. L. "Petrology of sedimentary rocks", Hemphill Publishing Company, 1974.

[22] ISRM "The Blue Book: the Complete ISRM Suggested Methods for Rock Characterization, Testing and Monitoring: 1974–2006", ISM Turkish National Group and the ISRM, 2007.

[23] ASTM "ASTM D2938-95 Standard Test Method for Unconfined Compressive Strength of Intact Rock Core Specimens", Advancing Standards Transforming Markets, West Conshohocken, PA, USA, 1995.
https://doi.org/10.1520/D2938-95

[24] ASTM "D2845-00 Standard Test Method for Laboratory Determination of Pulse Velocities and Ultrasonic Elastic Constants of Rock", Advancing Standards Transforming Markets International, West Conshohocken, PA, USA, 2000.
https://doi.org/10.1520/D2845-00

[25] Goodman, R. E. "Introduction to Rock Mechanics", John Wiley & Sons, Canada, 1989. ISBN 978-0471812005

[26] Breiman, L. "Bagging predictors", Machine learning, 24(2), pp.123–140. 1996.
https://doi.org/10.1007/BF00058655

[27] Cheng, B., Liu, X., Guo, K., Rastegarnia, A. "Investigating factors affecting the quality of water resources by multivariate analysis and soft computing approaches", Scientific Reports, 15(1), 28925, 2025.
https://doi.org/10.1038/s41598-025-13380-x

[28] Rumelhart, D. E., Durbin, R., Golden, R., Chauvin, Y., "Backpropagation: The basic theory", In: Backpropagation: Theory, architectures, and applications, L. Erlbaum Associates Inc. pp. 1–34, 1995.

[29] Cover, T., Hart, P. "Nearest neighbor pattern classification", IEEE transactions on Information Theory, 13(1), pp.21–27, 1967.
https://doi.org/10.1109/TIT.1967.1053964

[30] MathWorks Inc. "MATLAB, (R2019b)", [computer program] Available at: https://www.mathworks.com/?s_tid=gn_logo [Accessed: 05 February 2026]

[31] Brotons, V., Tomás, R., Ivorra, S., Grediaga, A., Martínez-Martínez, J., Benavente, D., Gómez-Heras, M. "Improved correlation between the static and dynamic elastic modulus of different types of rocks", Materials and Structures, 49(8), pp. 3021–3037, 2016.
https://doi.org/10.1617/s11527-015-0702-7

[32] Rastegarnia, A., Ghafoori, M., Moghaddas, N. H., Lashkaripour, G. R., Shojaei, H. "Application of cuttings to estimate the static characteristics of the dolomudstone rocks", Geomechanics and Engineering, 29(1), pp. 65–77, 2022.
https://doi.org/10.12989/gae.2022.29.1.065

[33] Brotons, V., Tomás, R., Ivorra, S., Grediaga, A. "Relationship between static and dynamic elastic modulus of calcarenite heated at different temperatures: The San Julián's stone", Bulletin of Engineering Geology and the Environment, 73(3), pp. 791–799, 2014.
https://doi.org/10.1007/s10064-014-0583-y

[34] Anon. O. H. "Classification of Rocks and Soils for Engineering Geological Mapping, Part 1: Rock and Soil Materials", Bulletin of the International Association of Engineering Geology, 19, pp. 364–437, 1979.

[35] Taylor, R. "Interpretation of the Correlation Coefficient: A Basic Review", Journal of Diagnostic Medical Sonography, 6(1), pp. 35–39, 1990.
https://doi.org/10.1177/875647939000600106

[36] Pereira, M. L., da Silva, P. F., Fernandes, I., Chastre, C. "Characterization and correlation of engineering properties of basalts", Bulletin of Engineering Geology and the Environment, 80(4), pp. 2889–2910, 2021.
https://doi.org/10.1007/s10064-021-02107-7

[37] Onaloa, D., Oloruntobi, O., Adedigba, S., Khan, F., James, L., Butt, S. "Static Young's modulus model prediction for formation evaluation", Journal of Petroleum Science and Engineering, 171, pp. 394–402, 2018.
https://doi.org/10.1016/j.petrol.2018.07.020

[38] Fei, W., Huiyuan, B., Jun, Y., Yonghao, Z. "Correlation of dynamic and static elastic parameters of rock", Electronic Journal of Geotechnical Engineering, 21(4), pp. 1551–1560, 2016.

[39] Kotsanis, D., Nomikos, P., Rozos, D. "Comparison of Static and Dynamic Young's Modulus of Prasinites", Materials Proceedings, 5(1), 54, 2021.
https://doi.org/10.3390/materproc2021005054

[40] Zheng, J., Shen, M., Motahari, M. R., Khajehzadeh, M. "Prediction of Rock Tensile Strength Using Soft Computing and Statistical Methods", Periodica Polytechnica Civil Engineering, 67(3), pp. 902–913, 2023.
https://doi.org/10.3311/PPci.22179

[41] Zhou, Z., Liu, N., Sun, Y., Wang, Z., Al Attabi, K. "Effect of textural and physical properties of the carbonate rocks on dynamic elastic modulus: application of statistical and intelligent methods", Physics and Chemistry of the Earth, Parts A/B/C, 139, 103964, 2025.
https://doi.org/10.1016/j.pce.2025.103964